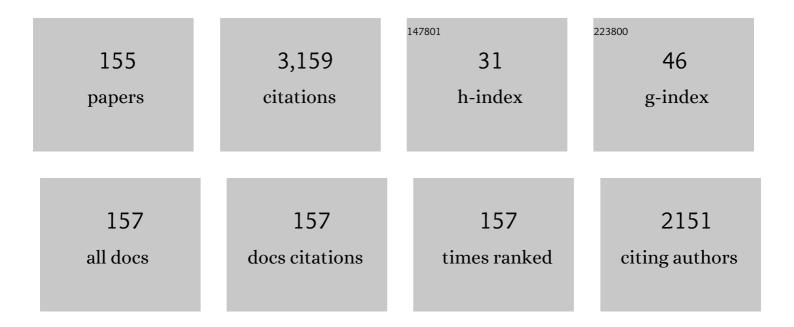
Lingfeng He

List of Publications by Year in descending order

Source: https://exaly.com/author-pdf/8504096/publications.pdf Version: 2024-02-01



LINCEENC HE

#	Article	IF	CITATIONS
1	<i>In Situ</i> Reaction Synthesis, Electrical and Thermal, and Mechanical Properties of Nb ₄ AlC ₃ . Journal of the American Ceramic Society, 2008, 91, 2258-2263.	3.8	112
2	Synthesis and structure–property relationships of a new family of layered carbides in Zr-Al(Si)-C and Hf-Al(Si)-C systems. Journal of the European Ceramic Society, 2013, 33, 2831-2865.	5.7	89
3	Physical and Mechanical Properties of Bulk Ta4AlC3Ceramic Prepared by an In Situ Reaction Synthesis/Hot-Pressing Method. Journal of the American Ceramic Society, 2007, 90, 2542-2548.	3.8	82
4	Corrosion behavior of an alumina forming austenitic steel exposed to supercritical carbon dioxide. Corrosion Science, 2014, 82, 67-76.	6.6	79
5	<i>In Situ</i> Reaction Synthesis and Mechanical Properties of V ₂ AlC. Journal of the American Ceramic Society, 2008, 91, 4029-4035.	3.8	78
6	First-principles prediction of the mechanical properties and electronic structure of ternary aluminum carbideZr3Al3C5. Physical Review B, 2006, 73, .	3.2	67
7	Synthesis and Characterization of Bulk Zr ₂ Al ₃ C ₄ Ceramic. Journal of the American Ceramic Society, 2007, 90, 3687-3689.	3.8	67
8	Effect of neutron irradiation on defect evolution in Ti3SiC2 and Ti2AlC. Journal of Nuclear Materials, 2016, 468, 194-206.	2.7	65
9	Atomic-scale microstructures of Zr2Al3C4 and Zr3Al3C5 ceramics. Acta Materialia, 2006, 54, 3843-3851.	7.9	63
10	Microstructure and properties of bulk Ta2AlC ceramic synthesized by an in situ reaction/hot pressing method. Journal of the European Ceramic Society, 2008, 28, 1679-1685.	5.7	63
11	Effects of neutron irradiation of Ti3SiC2 and Ti3AlC2 in the 121–1085°C temperature range. Journal of Nuclear Materials, 2017, 484, 120-134.	2.7	63
12	Synthesis, Physical, and Mechanical Properties of Bulk Zr3Al3C5Ceramic. Journal of the American Ceramic Society, 2007, 90, 1164-1170.	3.8	62
13	Thermal Conductivity in Nanocrystalline Ceria Thin Films. Journal of the American Ceramic Society, 2014, 97, 562-569.	3.8	58
14	Impact of irradiation induced dislocation loops on thermal conductivity in ceramics. Journal of the American Ceramic Society, 2019, 102, 7533-7542.	3.8	56
15	Atomic-scale microstructure and elastic properties of quaternary Zr–Al–Si–C ceramics. Acta Materialia, 2008, 56, 2022-2031.	7.9	54
16	In situ TEM observation of dislocation evolution in Kr-irradiated UO2 single crystal. Journal of Nuclear Materials, 2013, 443, 71-77.	2.7	51
17	Highly conductive and strengthened copper matrix composite reinforced by Zr2Al3C4 particulates. Scripta Materialia, 2009, 60, 976-979.	5.2	48
18	Crystal structure and theoretical elastic property of two new ternary ceramics Hf3Al4C6 and Hf2Al4C5. Scripta Materialia, 2008, 58, 679-682.	5.2	46

#	Article	IF	CITATIONS
19	Mechanical properties of Y2Ti2O7. Scripta Materialia, 2011, 64, 548-551.	5.2	42
20	Oxidation of Zr ₂ [Al(Si)] ₄ C ₅ and Zr ₃ [Al(Si)] ₄ C ₆ in air. Journal of Materials Research, 2008, 23, 3339-3346.	2.6	41
21	Mechanical properties and bioactivity of β-Ca2SiO4 ceramics synthesized by spark plasma sintering. Ceramics International, 2011, 37, 2459-2465.	4.8	41
22	Mechanical and Thermophysical Properties of Zr–Al–Si–C Ceramics. Journal of the American Ceramic Society, 2009, 92, 445-451.	3.8	40
23	Isothermal oxidation of bulk Zr ₂ Al ₃ C ₄ at 500 to 1000 °C in air. Journal of Materials Research, 2008, 23, 359-366.	2.6	39
24	High-temperature internal friction, stiffness and strength of Zr–Al(Si)–C ceramics. Scripta Materialia, 2009, 61, 60-63.	5.2	39
25	Microstructure changes and thermal conductivity reduction in UO2 following 3.9 MeV He2+ ion irradiation. Journal of Nuclear Materials, 2014, 454, 283-289.	2.7	38
26	Transient grating spectroscopy: An ultrarapid, nondestructive materials evaluation technique. MRS Bulletin, 2019, 44, 392-402.	3.5	37
27	Thermal Energy Transport in Oxide Nuclear Fuel. Chemical Reviews, 2022, 122, 3711-3762.	47.7	37
28	Corrosion-induced microstructural developments in 316 stainless steel during exposure to molten Li2BeF4(FLiBe) salt. Journal of Nuclear Materials, 2016, 482, 147-155.	2.7	36
29	In situ microstructural evolution in face-centered and body-centered cubic complex concentrated solid-solution alloys under heavy ion irradiation. Acta Materialia, 2020, 198, 85-99.	7.9	36
30	Microstructure and mechanical and thermal properties of ternary carbides in Hf–Al–C system. Acta Materialia, 2009, 57, 2765-2774.	7.9	33
31	High-Temperature Corrosion of UNS N10003 in Molten Li ₂ BeF ₄ (FLiBe) Salt. Corrosion, 2015, 71, 1257-1266.	1.1	33
32	Microstructure and microchemistry study of irradiation-induced precipitates in proton irradiated ZrNb alloys. Acta Materialia, 2019, 178, 228-240.	7.9	33
33	Elastic and thermal properties of Zr2Al3C4: Experimental investigations and <i>ab initio</i> calculations. Journal of Applied Physics, 2007, 102, .	2.5	32
34	The influence of lattice defects, recombination, and clustering on thermal transport in single crystal thorium dioxide. APL Materials, 2020, 8, .	5.1	32
35	Layered stacking characteristics of ternary zirconium aluminum carbides. Journal of Materials Research, 2007, 22, 3058-3066.	2.6	31
36	Microstructure evolution in Xe-irradiated UO2 at room temperature. Nuclear Instruments & Methods in Physics Research B, 2014, 330, 55-60.	1.4	31

#	Article	IF	CITATIONS
37	A New Method to Improve the Highâ€Temperature Mechanical Properties of Ti ₃ SiC ₂ by Substituting Ti with Zr, Hf, or Nb. Journal of the American Ceramic Society, 2010, 93, 1749-1753.	3.8	30
38	Ultrahigh-temperature oxidation of Zr2Al3C4 via rapid induction heating. Scripta Materialia, 2009, 60, 547-550.	5.2	29
39	Bubble formation and Kr distribution in Kr-irradiated UO2. Journal of Nuclear Materials, 2015, 456, 125-132.	2.7	29
40	α-U and ω-UZr2 in neutron irradiated U-10Zr annular metallic fuel. Journal of Nuclear Materials, 2020, 542, 152536.	2.7	28
41	<i>In Situ</i> Synthesis and Properties of Ti ₃ AlC ₂ /TiB ₂ Composites. Journal of the American Ceramic Society, 2007, 90, 3615-3620.	3.8	27
42	Real-time thermomechanical property monitoring during ion beam irradiation using in situ transient grating spectroscopy. Nuclear Instruments & Methods in Physics Research B, 2019, 440, 126-138.	1.4	27
43	Bridging the gap to mesoscale radiation materials science with transient grating spectroscopy. Physical Review B, 2016, 94, .	3.2	26
44	Subsurface imaging of grain microstructure using picosecond ultrasonics. Acta Materialia, 2016, 112, 209-215.	7.9	26
45	Self-healing behavior and strength recovery of ytterbium disilicate ceramic reinforced with silicon carbide nanofillers. Journal of the European Ceramic Society, 2019, 39, 3139-3152.	5.7	26
46	An integrated experimental and computational investigation of defect and microstructural effects on thermal transport in thorium dioxide. Acta Materialia, 2021, 213, 116934.	7.9	26
47	Radiation-induced grain subdivision and bubble formation in U3Si2 at LWR temperature. Journal of Nuclear Materials, 2018, 498, 169-175.	2.7	25
48	Combining mesoscale thermal transport and x-ray diffraction measurements to characterize early-stage evolution of irradiation-induced defects in ceramics. Acta Materialia, 2020, 193, 61-70.	7.9	25
49	Mechanisms and Kinetics of the Hydrothermal Oxidation of Bulk Titanium Silicon Carbide. Journal of the American Ceramic Society, 2010, 93, 1148-1155.	3.8	24
50	Microstructural characterization of annealed U-12Zr-4Pd and U-12Zr-4Pd-5Ln: Investigating Pd as a metallic fuel additive. Journal of Nuclear Materials, 2018, 502, 106-112.	2.7	23
51	Investigating corrosion behavior of Ni and Ni-20Cr in molten ZnCl2. Corrosion Science, 2021, 179, 109105.	6.6	22
52	Strengthening of a lithium disilicate glass-ceramic by rapid cooling. Ceramics International, 2018, 44, 11650-11657.	4.8	21
53	Phase and defect evolution in uranium-nitrogen-oxygen system under irradiation. Acta Materialia, 2021, 208, 116778.	7.9	21
54	Fullerene-like defects in high-temperature neutron-irradiated nuclear graphite. Carbon, 2020, 166, 113-122.	10.3	20

#	Article	IF	CITATIONS
55	Revealing 3D Morphological and Chemical Evolution Mechanisms of Metals in Molten Salt by Multimodal Microscopy. ACS Applied Materials & Interfaces, 2020, 12, 17321-17333.	8.0	20
56	On spinodal-like phase decomposition in U–50Zr alloy. Materialia, 2020, 9, 100592.	2.7	20
57	Experimental evidence for â€ ⁻ buckle, ruck and tuck' in neutron irradiated graphite. Carbon, 2020, 159, 119-121.	10.3	19
58	Dual Functional Ni ₃ S ₂ @Ni Core–Shell Nanoparticles Decorating Nanoporous Carbon as Cathode Scaffolds for Lithium–Sulfur Battery with Lean Electrolytes. ACS Applied Energy Materials, 2020, 3, 4173-4179.	5.1	19
59	Visualizing time-dependent microstructural and chemical evolution during molten salt corrosion of Ni-20Cr model alloy using correlative quasi in situ TEM and in situ synchrotron X-ray nano-tomography. Corrosion Science, 2022, 195, 109962.	6.6	19
60	Microstructure, mechanical, thermal, and oxidation properties of a Zr2[Al(Si)]4C5–SiC composite prepared by in situ reaction/hot-pressing. Journal of the European Ceramic Society, 2010, 30, 2147-2154.	5.7	18
61	Applications of Transient Grating Spectroscopy to Radiation Materials Science. Jom, 2015, 67, 1840-1848.	1.9	18
62	Strength improvement and purification of Yb ₂ Si ₂ O ₇ ‣iC nanocomposites by surface oxidation treatment. Journal of the American Ceramic Society, 2017, 100, 3122-3131.	3.8	18
63	Training artificial neural networks for precision orientation and strain mapping using 4D electron diffraction datasets. Ultramicroscopy, 2021, 231, 113256.	1.9	18
64	In Situ TEM Observation of Dislocation Evolution in Polycrystalline UO2. Jom, 2014, 66, 2553-2561.	1.9	17
65	Microstructure studies of interdiffusion behavior of U3Si2/Zircaloy-4 at 800 and 1000°C. Journal of Nuclear Materials, 2017, 486, 274-282.	2.7	17
66	Inferring radiation-induced microstructural evolution in single-crystal niobium through changes in thermal transport. Journal of Nuclear Materials, 2019, 523, 378-382.	2.7	17
67	Fuel-cladding chemical interaction of a prototype annular U-10Zr fuel with Fe-12Cr ferritic/martensitic HT-9 cladding. Journal of Nuclear Materials, 2021, 544, 152588.	2.7	17
68	Synthesis, Microstructure, and Mechanical Properties of Al ₃ BC ₃ . Journal of the American Ceramic Society, 2008, 91, 2343-2348.	3.8	16
69	A simple way to make pre-stressed ceramics with high strength. Journal of Materiomics, 2019, 5, 657-662.	5.7	16
70	Indirect characterization of point defects in proton irradiated ceria. Materialia, 2021, 15, 101019.	2.7	16
71	TEM characterization of dislocation loops in proton irradiated single crystal ThO2. Journal of Nuclear Materials, 2021, 552, 152998.	2.7	16
72	2.6MeV proton irradiation effects on the surface integrity of depleted UO2. Nuclear Instruments & Methods in Physics Research B, 2014, 319, 100-106.	1.4	15

#	Article	IF	CITATIONS
73	Determining oxidation states of transition metals in molten salt corrosion using electron energy loss spectroscopy. Scripta Materialia, 2021, 197, 113790.	5.2	15
74	Improving the high-temperature oxidation resistance of Zr2Al3C4 by silicon pack cementation. Journal of Materials Research, 2008, 23, 2275-2282.	2.6	14
75	<i>In situ</i> Reaction Synthesis and Mechanical Properties of TaC–TaSi ₂ Composites. International Journal of Applied Ceramic Technology, 2010, 7, 697-703.	2.1	14
76	Understanding spinodal and binodal phase transformations in U-50Zr. Materialia, 2021, 16, 101092.	2.7	14
77	Bubble evolution in Kr-irradiated UO2 during annealing. Journal of Nuclear Materials, 2017, 496, 242-250.	2.7	13
78	Non-contact, non-destructive mapping of thermal diffusivity and surface acoustic wave speed using transient grating spectroscopy. Review of Scientific Instruments, 2020, 91, 054902.	1.3	13
79	Development of a grain growth model for U3Si2 using experimental data, phase field simulation and molecular dynamics. Journal of Nuclear Materials, 2020, 532, 152069.	2.7	13
80	Electron microscopy characterization of fast reactor MOX Joint Oxyde-Gaine (JOG). Journal of Nuclear Materials, 2020, 531, 151964.	2.7	13
81	First principle studies of effects of solute segregation on grain boundary strength in Ni-based alloys. Journal of Alloys and Compounds, 2021, 874, 159795.	5.5	13
82	Low energy ion assisted deposition of Taâ^•Cu films. Journal of Applied Physics, 2007, 101, 024318.	2.5	12
83	Effect of Ti Dopant on the Mechanical Properties and Oxidation Behavior of Zr2[Al(Si)]4C5 Ceramics. Journal of the American Ceramic Society, 2011, 94, 1872-1877.	3.8	12
84	Synthesis of BN nanosheet/nanotube-Fe nanocomposites by pulsed wire discharge and high-temperature annealing. Materials Letters, 2014, 117, 120-123.	2.6	12
85	Irradiation effects in Generation IV nuclear reactor materials. , 2017, , 253-283.		12
86	Formation of tetragonal gas bubble superlattice in bulk molybdenum under helium ion implantation. Scripta Materialia, 2018, 149, 26-30.	5.2	12
87	STEM-EDS/EELS and APT characterization of ZrN coatings on UMo fuel kernels. Journal of Nuclear Materials, 2018, 511, 174-182.	2.7	12
88	In-situ TEM study of the ion irradiation behavior of U3Si2 and U3Si5. Journal of Nuclear Materials, 2018, 511, 56-63.	2.7	12
89	The correlation between microstructure and nanoindentation property of neutron-irradiated austenitic alloy D9. Acta Materialia, 2020, 195, 433-445.	7.9	12
90	Reciprocating Friction and Wear Behavior of Zr ₂ [Al(Si)] ₄ C ₅ and Zr ₂ [Al(Si)] ₄ C ₅ –SiC Composite Against Si ₃ N ₄ Ball. Journal of the American Ceramic Society, 2010, 93, 2369-2376.	3.8	11

#	Article	IF	CITATIONS
91	Microstructural characterization of as-cast U-20Pu-10Zr-3.86Pd and U-20Pu-10Zr-3.86Pd-4.3Ln. Journal of Nuclear Materials, 2018, 508, 310-318.	2.7	11
92	A transmission electron microscopy study of EBR-II neutron-irradiated austenitic stainless steel 304 and nickel-base alloy X-750. Journal of Nuclear Materials, 2020, 528, 151851.	2.7	11
93	Thermal conductivity of ThO2: Effect of point defect disorder. Journal of Applied Physics, 2021, 129, .	2.5	11
94	Dislocation loop evolution in Krâ€irradiated ThO ₂ . Journal of the American Ceramic Society, 2022, 105, 5419-5435.	3.8	11
95	Oxidation Behavior of Ternary Carbide Ceramics in Hf–Al–C System in Air. Journal of the American Ceramic Society, 2010, 93, 3427-3431.	3.8	10
96	Interdiffusion behavior of U3Si2 with FeCrAl via diffusion couple studies. Journal of Nuclear Materials, 2018, 502, 356-369.	2.7	10
97	Diffusion behaviors between metallic fuel alloys with Pd addition and Fe. Journal of Nuclear Materials, 2019, 525, 111-124.	2.7	10
98	Crystal Structure and Theoretical Elastic Property of a New Ternary Ceramic HfAl ₄ C ₄ . Journal of the American Ceramic Society, 2010, 93, 1164-1168.	3.8	9
99	Fabrication and Characterization of Tricalcium Silicate Bioceramics with High Mechanical Properties by Spark Plasma Sintering. International Journal of Applied Ceramic Technology, 2011, 8, 501-510.	2.1	9
100	Microstructural characterization of annealed U-20Pu-10Zr-3.86Pd and U-20Pu-10Zr-3.86Pd-4.3Ln. Journal of Nuclear Materials, 2019, 518, 287-297.	2.7	9
101	Enhanced Resistance to Irradiation Induced Ferritic Transformation in Nanostructured Austenitic Steels. Materialia, 2020, 13, 100806.	2.7	9
102	Preparation and strengthening mechanism of prestressed ceramic tile components. International Journal of Applied Ceramic Technology, 2022, 19, 604-611.	2.1	9
103	In situ monitoring of microstructure evolution during thermal processing of uranium-zirconium alloys using laser-generated ultrasound. Journal of Nuclear Materials, 2021, 553, 153005.	2.7	9
104	Effects of heat treatment on corrosion fatigue and stress corrosion crack growth of additive-manufactured Alloy 800H in high-temperature water. Corrosion Science, 2021, 191, 109739.	6.6	9
105	Intragranular thermal transport in U–50Zr. Journal of Nuclear Materials, 2020, 534, 152145.	2.7	9
106	Compositionally graded specimen made by laser additive manufacturing as a high-throughput method to study radiation damages and irradiation-assisted stress corrosion cracking. Journal of Nuclear Materials, 2022, 560, 153493.	2.7	9
107	Zirconium Aluminum Carbides: New Precursors for Synthesizing ZrO ₂ –Al ₂ O ₃ Composites. Journal of the American Ceramic Society, 2009, 92, 2751-2758.	3.8	8
108	Transmission Electron Microscopy Investigation of Krypton Bubbles in Polycrystalline CeO ₂ . Nuclear Technology, 2013, 182, 164-169.	1.2	8

#	Article	IF	CITATIONS
109	Listening to Radiation Damage In Situ: Passive and Active Acoustic Techniques. Jom, 2020, 72, 197-209.	1.9	8
110	Effect of proton pre-irradiation on corrosion of Zr-0.5Nb model alloys with different Nb distributions. Corrosion Science, 2020, 173, 108790.	6.6	8
111	Phase stability, mechanical properties, and ion irradiation effects in face-centered cubic CrFeMnNi compositionally complex solid-solution alloys at high temperatures. Journal of Nuclear Materials, 2022, 565, 153733.	2.7	8
112	Effect of Grain Boundaries on Krypton Segregation Behavior in Irradiated Uranium Dioxide. Jom, 2014, 66, 2562-2568.	1.9	7
113	Annealing-induced lattice recovery in room-temperature xenon irradiated CeO ₂ : X-ray diffraction and electron energy loss spectroscopy experiments. Journal of Materials Research, 2015, 30, 1555-1562.	2.6	7
114	Structure of the pellet-cladding interaction layer of a high-burnup Zr-Nb-O nuclear fuel cladding. Journal of Nuclear Materials, 2021, 556, 153196.	2.7	7
115	Thermal stability of helium bubble superlattice in Mo under TEM in-situ heating. Journal of Nuclear Materials, 2018, 505, 207-211.	2.7	6
116	Dislocation Loops in Proton Irradiated Uranium-Nitrogen-Oxygen System. Journal of Nuclear Materials, 2021, 557, 153244.	2.7	6
117	Inferring relative dose-dependent color center populations in proton irradiated thoria single crystals using optical spectroscopy. Physical Chemistry Chemical Physics, 2022, 24, 6133-6145.	2.8	6
118	Tribological Properties of a Zr ₂ Al ₃ C ₄ Ceramic at Ambient Temperature. Journal of the American Ceramic Society, 2009, 92, 141-146.	3.8	5
119	Mechanical and thermal properties of a Hf2[Al(Si)]4C5 ceramic prepared by in situ reaction/hot-pressing. Scripta Materialia, 2010, 62, 427-430.	5.2	5
120	Impact of small defects and dislocation loops on phonon scattering and thermal transport in <mml:math <br="" xmlns:mml="http://www.w3.org/1998/Math/MathML">altimg="si29.svg"><mml:mtp: 1998="" math="" mathml"<br="" www.w3.org="">altimg="si29.svg"><mml:mml="http: 1998="" math="" mathml"<br="" www.w3.org="">altimg="si29.svg"><mml:mml="http: 1998="" math="" mathml"<br="" www.w3.org="">altimg="si29.svg"><mml:mml="http: 1998="" math="" mathml"<br="" www.w3.org="">altimg="si29.svg"><mml:mml="http: 1998="" math="" mathml"<br="" www.w3.org="">altimg="si29.svg"><mml:mrow><mml:mtext>Th</mml:mtext><mml:msub><mml:msub>mathvariant="normal">>O<mml:mn>2</mml:mn></mml:msub></mml:msub></mml:mrow></mml:mml="http:></mml:mml="http:></mml:mml="http:></mml:mml="http:></mml:mtp:></mml:math> .	2.7	5
121	Journal of Nuclear Materials, 2022, 566, 153758. Nanoscale redistribution of alloying elements in high-burnup AXIOM-2 (X2®) and their effects on in-reactor corrosion. Corrosion Science, 2021, 190, 109652.	6.6	4
122	The dynamic evolution of swelling in nickel concentrated solid solution alloys through inÂsitu property monitoring. Applied Materials Today, 2021, 25, 101187.	4.3	4
123	Raman and photoluminescence evaluation of ion-induced damage uniformity in ThO2. Nuclear Instruments & Methods in Physics Research B, 2022, 515, 69-79.	1.4	4
124	Unraveling small-scale defects in irradiated ThO2 using kinetic Monte Carlo simulations. Scripta Materialia, 2022, 214, 114684.	5.2	4
125	Fission Products in Nuclear Fuel: Comparison of Simulated Distribution with Correlative Characterization Techniques. Microscopy and Microanalysis, 2013, 19, 968-969.	0.4	3
126	Hydrothermal synthesis of silicon oxide clad uranium oxide nanowires. Journal of the American Ceramic Society, 2018, 101, 1004-1008.	3.8	3

#	Article	IF	CITATIONS
127	Degradation mechanism of lead-vanado-iodoapatite in NaCl solution. Corrosion Science, 2020, 172, 108720.	6.6	3
128	Early-stage microstructural evolution and phase stability in neutron-irradiated ferritic-martensitic steel T91. Journal of Nuclear Materials, 2021, 557, 153207.	2.7	3
129	Chemical and elemental mapping of spent nuclear fuel sections by soft X-ray spectromicroscopy. Journal of Synchrotron Radiation, 2022, 29, 67-79.	2.4	3
130	A Square Pulse Thermoreflectance Technique for the Measurement of Thermal Properties. International Journal of Thermophysics, 2022, 43, 1.	2.1	3
131	Thermal conductivity reduction in (Zr _{0.25} Ta _{0.25} Nb _{0.25} Ti _{0.25})C high entropy carbide from extrinsic lattice defects. Materials Research Letters, 2022, 10, 611-617.	8.7	3
132	Effect of thin strain-compensated Al0.6Ga0.4P layers on the growth of multiple-stacked InP/In0.5Al0.3Ga0.2P quantum dots. Journal of Electronic Materials, 2006, 35, 701-704.	2.2	2
133	Impact of krypton irradiation on a single crystal tungsten: Multi-modal X-ray imaging study. Scripta Materialia, 2020, 188, 296-301.	5.2	2
134	Phase stability and microstructural evolution in neutron-irradiated ferritic-martensitic steel HT9. Journal of Nuclear Materials, 2021, 557, 153252.	2.7	2
135	Acoustic mapping by picosecond ultrasonics for elastic property measurement: Experimental demonstration on a TRISO fuel compact. Journal of Nuclear Materials, 2022, 558, 153391.	2.7	2
136	Sensitization, desensitization, and carbide evolution of Alloy 800H made by laser powder bed fusion. Additive Manufacturing, 2022, 50, 102547.	3.0	2
137	Synthesis and Characterization of Uranium Trichloride in Alkali-Metal Chloride Media. Journal of Nuclear Materials, 2022, , 153728.	2.7	2
138	Measurement of grain boundary strength of Inconel X-750 superalloy using in-situ micro-tensile testing techniques in FIB/SEM system. Materials Science & Engineering A: Structural Materials: Properties, Microstructure and Processing, 2022, 849, 143475.	5.6	2
139	Surface strengthening of Ti3SiC2 through magnetron sputtering of Mo and Zr and subsequent annealing. Journal of the European Ceramic Society, 2010, 30, 2123-2130.	5.7	1
140	Inert Gas Measurement of Single Bubble in CeO2. Microscopy and Microanalysis, 2015, 21, 751-752.	0.4	1
141	Atom Probe Tomography for Burnup and Fission Product Analysis for Nuclear Fuels. Microscopy and Microanalysis, 2020, 26, 3086-3088.	0.4	1
142	Proton irradiation-induced blistering in UO2. MRS Advances, 0, , 1.	0.9	1
143	Fluctuation Electron Microscopy Study of Medium-Range Packing Order in Ultrastable Indomethacin Glass Thin Films. Materials Research Society Symposia Proceedings, 2015, 1757, 32.	0.1	0
144	Challenges and Opportunities on Elucidating Irradiated Fuels with Atom Probe Tomography. Microscopy and Microanalysis, 2018, 24, 2206-2207.	0.4	0

#	Article	IF	CITATIONS
145	Erratum to Interdiffusion Behavior of U3Si2 with FeCrAl via Diffusion Couple Studies J. Nucl. Mater. 502 (2018) 356–369. Journal of Nuclear Materials, 2018, 507, 403-417.	2.7	0
146	Metallic Fast Reactor Separate Effect Studies for Fuel Safety. Journal of Nuclear Engineering and Radiation Science, 2021, 7, .	0.4	0
147	Isotopic Analysis of Irradiated Ceramic Fuel for Burnup and Microchemical Assessment Using Atom Probe Tomography Microscopy and Microanalysis, 2021, 27, 416-417.	0.4	0
148	Machine Learning Based Precision Orientation and Strain Mapping from 4D Diffraction Datasets. Microscopy and Microanalysis, 2021, 27, 1276-1278.	0.4	0
149	Advanced Characterization of Additively Manufactured 316L Stainless Steel for Nuclear Applications. Microscopy and Microanalysis, 2021, 27, 2160-2161.	0.4	0
150	On Spinodal-Like Phase Decomposition in U-50 Zr Alloy. SSRN Electronic Journal, 0, , .	0.4	0
151	Fuel-Cladding Chemical Interaction of a Prototype Annular U-10Zr Fuel with Fe-12Cr Ferritic/Martensitic Cladding. SSRN Electronic Journal, 0, , .	0.4	0
152	In Situ Microstructural Evolution in Fcc and Bcc Complex Concentrated Solid-Solution Alloys Under Heavy Ion Irradiation. SSRN Electronic Journal, 0, , .	0.4	0
153	Interdiffusion Behavior of FeCrAl with U3Si2. Minerals, Metals and Materials Series, 2018, , 175-184.	0.4	0
154	Investigating the Effect of CrCl3 on Corrosion Behavior of Ni and Ni-20Cr in Molten ZnCl2 Salt By Electrochemical Noise Measurements. ECS Meeting Abstracts, 2020, MA2020-02, 2923-2923.	0.0	0
155	4D in Situ Temperature-Dependent Study on Morphological and Chemical Evolution of Metals in Molten Salt Environments By Multimodal Microscopy. ECS Meeting Abstracts, 2020, MA2020-02, 2925-2925.	0.0	0